Robust and Efficient Screen-Printed Molecular Anodes with Anchored Water Oxidation Catalysts

Robin Dürr, Sirikorn Chasvised, Marcos Gil-Sepulcre, Andrew Howe, Md Asmaul Hoque, Van N'guyen, Saeed Sadeghi, Stephanie Reynaud, Cyril Cugnet, Laurent Authier, et al.

Robust and Efficient Screen-Printed Molecular Anodes with Anchored Water Oxidation Catalysts

Robin Dürr[a,†], Sirikorn Chasvised[b,c,†], Marcos Gil Sepulcre[a], Andrew Howe[a,b,c], Md Asmaul Hoque[a], Van N'Guyen[b,c], Saeed Sadhegi[b,c], Stephanie Reynaud[b], Cyril Cugnet[b], Laurent Authier[b], Carolina Gimbert-Suriñach[d], Antoine Bousquet [b*], Antoni Llobet[a,d*], Laurent Billon[b,c*]

[a] Institute of Chemical Research of Catalonia (ICIQ), Barcelona Institute of Science and Technology (BIST). Av. Països Catalans 16, 43007 Tarragona, Spain.

[b] Universite de Pau et Pays de l'Adour, E2S UPPA, CNRS, Institut des Sciences Analytiques & de PhysicoChimie pour l'Environnement & les Matériaux, UMR5254, 64000 Pau, France.

[b] Bio-inspired Materials group: Functionalities & Self-assembly, UPPA, 64000 Pau, France.

[d] Departament de Química, Universitat Autònoma de Barcelona. Cerdanyola del Valles, 08193 Barcelona, Spain.

[†] These authors contributed equally to this work.

Corresponding authors:

antoine.bousquet@univ-pau.fr

allobet@iciq.cat

laurent.billon@univ-pau.fr

ABSTRACT

In this work, we present the preparation of highly stable and active screen-printed anodes for electrochemical water splitting in neutral media. With the combination of printed electrodes and molecular water oxidation catalyst, we successfully take advantage of a low-cost and up-scalable fabrication method of graphitic electrodes with the outstanding catalytic activity and stability of oligomeric ruthenium based molecular water oxidation catalysts, offering a promising electro-anode for water oxidation applications.

GRAPHICAL ABSTRACT

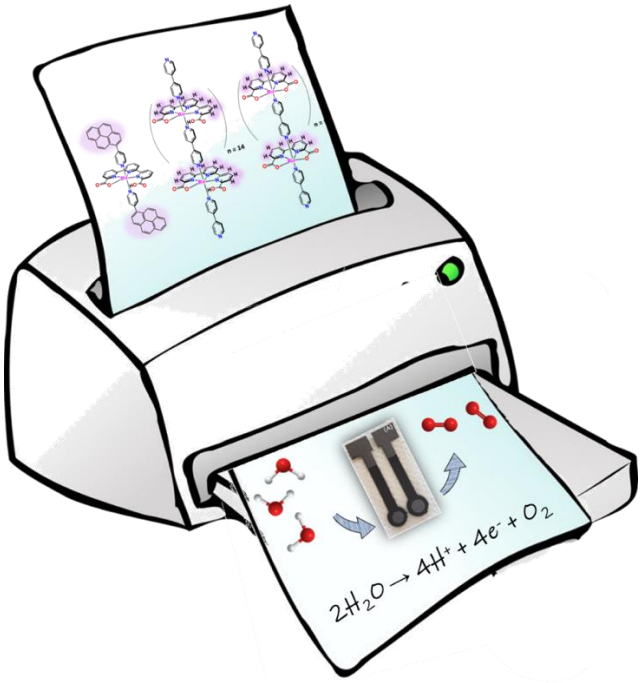

Keywords

Screen printing, molecular electrodes, water oxidation, Ru complexes, water splitting

1. Introduction

The impact of fossil fuel usage in our modern societies have urged the scientific community to find alternative fuels that can sustain current energy demands using carbon-neutral, clean and sustainable sources.[1,2,3,4] Inspired by nature, artificial photosynthesis aims at capturing and storing the energy from solar photons into chemical bonds, generating clean and sustainable fuels, that obtained in this manner are termed solar fuels.[5,6,7,8] Light-induced water splitting (*hυ*-WS), where the energy from sunlight is stored into H-H and O-O bonds, can be considered a model case.[9,10] Nevertheless, many scientific challenges still need to be overcome to be able to implement *hυ*-WS as a widespread technology. Among them are the need to improve the performance of low-cost catalysts in terms of efficiency and stability, as well as their capacity to harmoniously interact with the light absorber.[11]

One of the crucial issues that needs to be solved in *hυ*-WS, is the need to have access to an efficient and robust Water Oxidation Catalyst (WOC) that can be easily incorporated into rugged electrodes. The water oxidation reaction is particularly challenging because it involves the removal of four electrons and four protons from two water molecules and the formation of an O-O bond.[12,13] Furthermore, it is a thermodynamically unfavorable reaction with a formal redox potential of 1.23 V vs. NHE at pH 0.[14] From a molecular perspective, the best WOCs described up to now are based on Ru complexes coordinated with Flexible Adaptive Multidentate Equatorial (FAME) ligands,[15] including the family of Ru-tda and Ru-bda coordination complexes.[16,17,18,19,20,21] To incorporate these catalysts into technologically useful devices based on photoelectrochemical (PEC) cells, they must be anchored on conductive and/or semi-conductive surfaces so that efficient molecular (photo)anodes can be developed.[22,23] From this point of view, the choice of the anchoring strategy is essential because it simplifies the construction engineering as opposed to use the catalysts in homogeneous phase.[24] So far, several strategies have been developed for the anchoring of WOCs onto surfaces that include covalent bonding,[25,26,27,28,29] polymerization into insoluble but conductive polymers[24] and supramolecular interactions such as CH-π[30,31] and π-π.[32,33]

In addition, the possibility of using the screen-printing processing technologies[34] to generate electro-anodes and cathodes makes it highly attractive to advanced applications for PECs because it simplifies its construction and thus it also reduces its costs.

Here on, we describe the use of a screen-printing technique in order to easily prepare electrode-anodes containing molecular WOCs based on monomeric and oligomeric Ru complexes suitable to perform water oxidation catalysis.

2. Results and Discussion

2a. Screen-printed electrodes

A commercial triblock copolymer Poly(Methyl MethAcrylate)-*b*-Poly(*n*-Butyl Acrylate)-*b*-Poly(Methyl MethAcrylate) (MBM) is used as a matrix to bind graphite powder to generate an ink containing mesitylene or *o*-xylene as solvent, that can be used as a scaffold to immobilize carbon nanotubes supported ruthenium catalyst (WOC@CNT) and presenting a high affinity with the perfluorinated NAFION membrane.[35,36] The preparation of screen-printed electrodes consisted on using a polymeric Nafion or high impact polymeric styrene (HIPS) substrate[37] as support where the conductive ink was printed . After solvent evaporation, a molecular water oxidation catalyst anchored on multi walled carbon nanotubes (MWCNTs or CNTs) is deposited, generating a molecular anode (Figure 1A). Further, an easily up-scalable screen-printing methodology was developed to provide flexible electrode coated on NAFION proton membrane.

To prepare the electrodes, several parameters were optimized such as MBM/graphite ratio, the solvent used during the ink preparation and the number of printed layers (Table 1). The characterization of these new electrodes included the measurement of their film thickness and porosity, their conductivity and their electrochemical response through evaluation of peak-to-peak separation for the ferrocene/ferrocenium (III/II) redox couple, used as internal standard. The main results obtained from these experiments are gathered in Table 1. The best electrode in terms of conductivity and film thickness turn out to be prepared with MBM/Graphite (40:60), also labeled as "**PE**" (for printed electrode), and thus was the one used throughout this work unless explicitly mentioned (Table 1, entry 4).

2b. Anchoring of Ru WOCs on PE and redox properties.

In order to obtain powerful anodes for the water oxidation reaction, the next step involved the anchoring of molecular WOCs onto the PE described above. For this purpose, we used a family of monomeric and oligomeric Ru-based molecular of WOCs that were anchored *via* π-π stacking interactions or *via* CH-π interactions on graphitic surfaces. Therefore, we choose the WOC [Ru(tda)(pyp)$_2$], **1,** (tda^{2-} is [2,2':6',2''-terpyridine]-6,6''-dicarboxylate and *pyp* is 4-(pyrene-1-yl)pyridine) containing a pyrene functionality that strongly attaches to graphitic surface *via* π-π interactions. We further chose {[Ru(bda)(bpy)]$_{10}$(μ-bpy)}, **10,** (*bda* is 2,2'-bipyridine-6,6'-dicarboxylate; *bpy* is 4,4'-bipyridine) and {[Ru(tda)(bpy)]$_{15}$(μ-bpy)}, **15**, which are capable to form CH-π interactions with graphitic surfaces through hydrogens of the equatorial ligand

backbone (see Figure 1B for a drawing of WOCs). All these complexes were prepared following the methods previously described in the literature.[30,32] The catalysts were then anchored on CNTs by mixing a solution of the corresponding WOC and a sonicated suspension of the CNT (See supporting information for details and Figure S1) to generate the WOC@CNT. This hybrid material was sequentially dried and mixed with methanol, and subsequently drop casted onto the PE, forming the WOC@CNT@PE molecular printed electrodes (MPE), that will be used as water oxidation anodes, as outlined in Figure 1C. The prepared hybrid MPE are named **1@CNT@PE**, **10@CNT@PE** and **15@CNT@PE** depending of contained WOC. The Ru loading (*Γ*) at the surface of the electrode ranges from 0.5 to 9 nmol/cm^2 (Table 2), depending on the catalyst and on the anchoring strategy. It is interesting to realize here that, as shown in the Table 2, the anchoring through aromatic CH-π interaction can generate a mass deposition up to 18 times higher than the π-π staking interaction.

The electrocatalytic performance of the molecular electrodes was tested in a three-electrode half-cell configuration with a 1.0 M phosphate buffer (pH 7). The electrochemical analysis is based on Cyclic Voltammetry (CV) (Figure S4), Differential Pulse Voltammetry (DPV) (Figure S3) and controlled potential-current techniques. The molecular printed electrodes (WOC@CNT@PE) were used as working electrode (WE), a platinum mesh was employed as counter electrode (CE) and a Hg/Hg_2SO_4 (K_2SO_4 sat.) electrode was used as reference (RE). All potentials were converted to NHE by adding 0.65 V to the measured potential. Before usage, the uncompensated resistance of the electrode was determined for all the MPEs prepared in this work, following the CHI potentiostat iR compensation routine. It is important to realize here that the combination of printed electrodes, CNTs and catalysts gives resistances that are two to three orders of magnitude larger than for instance typical glassy carbon disk electrodes with immobilized hybrid molecular Ru-based catalysts, anchored to CNTs via CH-π interactions. This increase in resistance is mainly due to the low conductivity of the ink generated, which contains a combination of graphitic material (highly conductive) with the MBM binder that is a non-electrically conductive polymer. The limited conductivity of the overall screen-printed molecular anode, will only affect to redox processes where large current densities are involved, particularly the electrocatalytic waves, as will be discussed in the next section. An additional consequence of these large electrode resistances is the decrease on the measured TOF_{max} (k_{obs}), by one to two orders of magnitude as compared to their counterparts in homogeneous phase or anchored on graphitic electrodes.[16,30,32] The TOF_{max} values for **1@CNT@PE**, **10@CNT@PE** and **15@CNT@PE** were measured by using Foot of the Wave Analysis (FOWA),[38] are in the range of 396 – 2646 s^{-1} as indicated in Table 2 (Figures S10-12).

The CV of **1@CNT@PE** showed the typical Ru^{III}/Ru^{II} and Ru^{IV}/Ru^{III} redox couples at $E_{1/2}$ = 0.61V (ΔE = 100 mV) and $E_{1/2}$ = 1.05 V (ΔE = 70 mV) respectively as can be observed in Figure 2A. In case of **15@CNT@PE** the Ru^{III}/Ru^{II} and Ru^{IV}/Ru^{III} redox couples are visible at $E_{1/2}$ = 0.67 V (ΔE = 230 mV) and $E_{1/2}$ = 1.13 V (ΔE = 260 mV), respectively (Figure 2B), which is in accordance with previously reported values.[16,30,32] For the **10@CNT@PE** the Ru^{III}/Ru^{II} redox couple is detected at $E_{1/2}$ = 0.66 V (ΔE = 200 mV) and the redox potential of Ru^{IV}/Ru^{III} is visible at $E_{1/2}$ = 0.83 V (ΔE = 170 mV) (Figure 2C). Additionally, a third oxidation (Ru^{V}/Ru^{IV}) that appears at 1.2 V is noted, which is related to water oxidation to dioxygen. Complexes **1** and **15** are not water oxidation catalyst but precursors to active catalysts and thus they need an activation step to generate the indispensable Ru-OH_2 group. On the other hand, complex **10** readily coordinates a water molecule in presence of aqueous solutions and therefore catalyzes water oxidation already in the first scan.[19,39] It is important to point out here that once anchored on a graphitic surface and with repetitive CV scans in the potential range of the catalytic wave, **10** additionally coordinates a second water molecule, generating the more active Ru-$(OH_2)_2$ species. The presence of this new species can be easily monitored by CV and DPV and shows three redox couples at 0.59 V (Ru^{III}/Ru^{II}), 0.74 V (Ru^{IV}/Ru^{III}) and 0.92 V (Ru^{V}/Ru^{IV}) together with a large electrocatalytic wave in the range of 1.2-1.3 V (Figure 2C and Figures S3 and 4). In case of **1@CNT@PE** and **15@CNT@PE**, the activation is carried out *via* Chronoamperometry (CA; also named as Controlled Potential Electrolysis, CPE, or Bulk Electrolysis, BE), at E_{app} = 1.32 V for 1000 s in a pH 11.6 phosphate buffer (phbf) solution (see Figure S2 for additional details). This generates new redox features that are due to the redox couples Ru^{III}/Ru^{II} at $E_{1/2}$ = 0.62 V (ΔE = 60 mV) and Ru^{IV}/Ru^{III} at $E_{1/2}$ = 0.8 V (ΔE = 100 mV) for **1-H_2O@CNT@PE** and $E_{1/2}$ = 0.59 V (ΔE =190 mV) and $E_{1/2}$ = 0.87 V (ΔE = 370 mV) for **15-H_2O@CNT@PE**.[16,30] In both cases, a new large electrocatalytic wave assigned to water oxidation appears in the range of 1.2-1.3 V.

2c. Long term performance of MPE

To test the long term stability under different working conditions a series of Chronopotentiometries (CP) and Chronoamperometries (CA) were carried out for **1-H_2O@CNT@PE**, **15-H_2O@CNT@PE** and **10-$(H_2O)_2$@CNT@PE** and the results are reported in Figure 3 and Figures S5-9. The figure 3 shows the CP obtained setting a constant current of 25, 50, 100, 125, 175 and 225 μA (J = 0.13-1.15 mA·cm^2) for two hours each at pH 7 (1 M phbf). From 25 to 175 μA the three molecular electrodes are very stable over the 2 h period tested. However, the potentials needed to reach the corresponding current intensity are always lower for **10** and

15 than for **1**. In the case of i_{app} = 25 μA, the potentials needed are 1.25, 1.31 and 1.42 V for **15-H_2O@CNT@PE**, **10-$(H_2O)_2$@CNT@PE** and **1-H_2O@CNT@PE** respectively, while the blank that involves the use of CNT as a WOC appears at 1.75 V. For **1-H_2O@CNT@PE** and **15-H_2O@CNT@PE**, since the active site is similar as is the uncompensated resistance, the 150 mV difference can be associated with the much larger catalyst loading deposited at the surface of the electrode that is about 18 times larger for **15-H_2O@CNT@PE** (9.1 nmols/cm^2) than for **1-H_2O@CNT@PE** (0.5 nmols/cm^2). Accordingly, this potential difference increases as the current set, is increased up to 175 μA where it reaches a difference value of 300 mV. It is interesting to see that upon increasing the set current densities, the electrodes need to increases the applied potential accordingly. However, the increase of required potential for **10-$(H_2O)_2$@CNT@PE** for increased current is smaller than for **15-H_2O@CNT@PE** and this generates a crossing potential at 100 μA. This smaller increase is mainly due to much lower resistivity of **10-$(H_2O)_2$@CNT@PE** with regard to **15-H_2O@CNT@PE**. It is also interesting to see that the CNT at low current densities can achieve relatively stable water oxidation catalysis but above 50 μA there is a clear deviation from linearity indicating electrode oxidation. In these experiments, assuming 100% Faradaic Efficiency (FE) according to reported values in the literature,[30,32] the number of TONs achieved are 7.300, 144.800 and 92.200 for **15-H_2O@CNT@PE**, **10-$(H_2O)_2$@CNT@PE** and **1-H_2O@CNT@PE** respectively, that clearly outlines the robustness of the present MPEs.

To evaluate the integrity of the catalyst on the previously presented CP experiments, a CV was carried out every two hours and these results are exhibited in Figure 4. On the right-hand side, a plot of the catalytic current density at 1.45 V as well as the loading of Ru, after each CP experiment is displayed for **15-H_2O-tda-bpy@CNT@PE**. It can be graphically observed that as the catalyst loading progressively decrease, the catalytic current remains constant. The fact that the catalytic current is independent of catalyst loading indicates that the current density is limited by the overall conductivity of the electrode material. This is also clearly manifested with CV shape of the present electrode in comparison of the catalyst behavior directly anchored on a highly conductive surface such as a glassy carbon electrode, as mentioned above.[30] The mass de-anchoring during CP experiments is associated with the de-anchoring of the CNT from the PE and/or the de-anchoring of the WOC from the CNTs. The fact that no new species appear during CVs used to monitor the whole process discards the presence of degrading pathways for the molecular catalyst.

A similar CV monitoring of the CP experiment was also carried out for **10-$(H_2O)_2$@CNT@PE** and the results are shown in Figure 5. As observed in the Γ vs. t (i_{app}) plot, there seems to be a process of oligomeric reorganization within the CNT, that increases the number of active sites

accessibility to the electrode as the CP proceeds up to 125 μA where it then becomes constant. An additional long term CP experiment was carried out at 100 μA for 20 h for **10-(H_2O)$_2$@CNT@PE** and **15-(H_2O)@CNT@PE**, that again showed a stable behavior over the whole experiment (Figure S8 and Table 2), with *E* values of 1.36 and 1.65 V and TONs of TONs of 39.800 and 15.500, respectively. Finally, a CA experiment was carried out for **15-(H_2O)@CNT@PE** at a constant E_{app} = 1.45 V for 20 h, again showing a high stability achieving more than 58.100 TONs (Table 2)

3. Conclusions

Herein, we have shown the viability constructing flexible molecular screen-printed electrodes MPEs based on the MBM binder for conductive graphite and adhesive for Nafion membrane in view of a use as membrane electrode assembly in a water splitting device. We described their performance, after the immobilization of a catalyst, as a molecular electro-anode for water oxidation catalysis. The catalyst anchoring has been carried out *via* supramolecular CH-π and π-π interactions showing an exceptional stability during turnover. This anchoring achieves a large degree of surface coverage and is preferred to covalent bonding since no additional functionalization is needed in the case of CH-π interaction. In addition, it does not require the modification of the graphitic surfaces that can lead to a reduce conductivity of the latter.

The overall performance of the electro-anode has been monitored based on electrochemical techniques and display long term stability for 12-20 h reaching TON values of 144.800 in case of **10-(H_2O)$_2$@CNT@PE**. The current densities achieved by the MPE are mainly limited by the overall conductivity of the MPE and not by the surface coverage or the intrinsic activity of the WOC. If higher current densities were needed then more conductive binders or mixing of binders/graphite would be required. Over long catalytic periods of time, the loading of the electrode slowly but progressively decreases due to the de-anchoring of the CNTs from the screen-printed electrode. The possibility of including highly porous graphitic materials where the catalyst could be anchored beforehand will substantially increase its stability.

In conclusion, we have demonstrated the viability of generating robust and efficient MPEs, which still lots of room for improvement but that can already be used for their implementation into printed PECs.

Supporting Information

Additional details on the preparation of printed electrodes and complementary electrochemical experiments.

Acknowledgments

Support from Ministerio de Ciencia, Innovacion y Universidades and FEDER (PID2019-111617RB-I00), AGAUR 2017-SGR-1631, Ministerio de Ciencia e Innovacion for a Severo Ochoa Excellence Accreditation grant 2020-2023 (CEX2019-000925-S, MIC/AEI)" and EU-funded ITN eSCALED (Grant agreement ID: 765376) are gratefully acknowledged.

References

(1) Lewis, N. S. Research Opportunities to Advance Solar Energy Utilization. *Science*. 2016.

(2) Ventosa, M.; Oliveras, J.; Bastús, N. G.; Gimbert-Suriñach, C.; Puntes, V.; Llobet, A. Nanocrystal-Molecular Hybrids for the Photocatalytic Oxidation of Water. *ACS Appl. Energy Mater.* **2020**, 3, 10008-10014.

(3) Steffen, W.; Rockström, J.; Richardson, K.; Lenton, T. M.; Folke, C.; Liverman, C.; Summerhayes, C. P.; Barnosky, A. D.; Cornell, S. E.; Crucifix, M.; Donges, J. F.; Fetzer, I.; Lade, S. J.; Scheffer, M.; Winkelmann, R.; Schellnhuber, H. J. *Proc. Natl. Acad. Sci. USA* **2018**, *115*, 8252-8259.

(4) Balmaseda, M. A.; Trenberth, K. E.; Källén, E. Distinctive climate signals in reanalysis of global ocean heat content. *Geophys. Res. Lett.* **2013**, *40*, 1754-1759.

(5) Nocera, D. G. The Artificial Leaf. *Acc. Chem. Res.* **2012**, *45*, 767–776.

(6) Kärkäs, M. D.; Verho, O.; Johnston, E. V.; Åkermark, B. Artificial Photosynthesis: Molecular Systems for Catalytic Water Oxidation. *Chemical Reviews*. **2014**, *114*, 11863–12001.

(7) House, R. L.; Iha, N. Y. M; Coppo, R. L.; Alibabaei, L.; Sherman, B. D.; Kang, P.; Brennaman, M. K.; Hoertz, P. G.; Meyer T. J. Artificial photosynthesis: Where are we now? Where can we go? *J. Photochem. Photobiol. C: Photochem. Rev.* **2015**, *25*, 32–45.

(8) Dogutan, D. K.; Nocera, D. G. Artificial Photosynthesis at Efficiencies Greatly Exceeding That of Natural Photosynthesis. *Acc. Chem. Res.* **2019**, *52*, 3143−3148.

(9) Berardi, S.; Drouet, S.; Francàs, L.; Gimbert-Suriñach, C.; Guttentag, M.; Richmond, C.; Stoll, T.; Llobet, A. Molecular Artificial Photosynthesis. *Chem. Soc. Rev*. **2014**, *43*, 7501–7519.

(10) Sala, X.; Maji, S.; Bofill, R.; García-Antón, J.; Escriche, L.; Llobet, A. Molecular Water Oxidation Mechanisms Followed by Transition Metals: State of the Art. *Acc. Chem. Res.* **2014**, *47*, 504–516.

(11) Garrido-Barros, P.; Gimbert-Suriñach, C.; Matheu, R.; Sala, X.; Llobet, A. How to Make an Efficient and Robust Molecular Catalyst for Water Oxidation. *Chem. Soc. Rev*. **2017**, *46*, 6088–6098.

(12) Shaffer, D. W.; Xie, Y.; Concepcion, J. J. O-O Bond Formation in Ruthenium-Catalyzed Water Oxidation: Single-Site Nucleophilic Attack: Vs. O-O Radical Coupling. *Chem. Soc. Rev*. **2017**, *46*, 6170–6193.

(13) Tahir, M.; Pan, L.; Idrees, F.; Zhang, X.; Wang, L.; Zou, J. J.; Wang, Z. L. Electrocatalytic Oxygen Evolution Reaction for Energy Conversion and Storage: A Comprehensive Review. *Nano Energy*. **2017**, *37*, 136–157.

(14) Schalenbach, M.; Zeradjanin, A. R.; Kasian, O.; Cherevko, S.; Mayrhofer, K. J. J. A Perspective on Low-Temperature Water Electrolysis - Challenges in Alkaline and Acidic Technology. *Int. J. Electrochem. Sci.* **2018**, *16*, 1173–1226.

(15) Matheu, R.; Ertem, M. Z.; Gimbert-Suriñach, C.; Sala, X.; Llobet, A. Seven Coordinated Molecular Ruthenium–Water Oxidation Catalysts: A Coordination Chemistry Journey. *Chem. Rev.* **2019**, *119*, 3453-3471.

(16) Matheu, R.; Ertem, M. Z.; Benet-Buchholz, J.; Coronado, E.; Batista, V. S.; Sala, X.; Llobet,

A. Intramolecular Proton Transfer Boosts Water Oxidation Catalyzed by a Ru Complex. *J. Am. Chem. Soc.* **2015**, *137*, 10786-10795.

(17) Matheu, R.; Garrido-Barros, P.; Gil-Sepulcre, M.; Ertem, M. Z.; Sala, X.; Gimbert-Suriñach, C.; Llobet, A. The Development of Molecular Water Oxidation Catalysts. *Nat. Rev. Chem.* **2019**, *3*, 331–341.

(18) Duan, L.; Fischer, A.; Xu, Y.; Sun, L. Isolated Seven-Coordinate Ru(IV) Dimer Complex with [HOHOH]− Bridging Ligand as an Intermediate for Catalytic Water Oxidation. *J. Am. Chem. Soc.* **2009**, *131*, 10397-10399.

(19) Duan, L.; Bozoglian, F.; Mandal, S.; Steward, B.; Privalov, T.; Llobet, A.; Sun, L. A molecular ruthenium catalyst with water-oxidation activity comparable to that of photosystem II. *Nat. Chem.* **2012**, *4*, 418-423.

(20) Zhang, B.; Sun, L. Ru-bda: Unique Molecular Water-Oxidation Catalysts with Distortion Induced Open Site and Negatively Charged Ligands. *J. Am. Chem. Soc.* **2019**, *141*, 5565−5580.

(21) Matheu, R.; Ertem, M. Z.; Gimbert-Suriñach, C.; Benet-Buchholz, J.; Sala, X.; Llobet, A. Hydrogen Bonding Rescues Overpotential in Seven-Coordinated Ru Water Oxidation Catalysts. *ACS Catal.* **2017**, *7*, 6525-6532.

(22) Matheu, R.; Moreno-Hernandez, I. A.; Sala, X.; Gray, H. B.; Brunschwig, B. S.; Llobet, A.; Lewis, N. S. Photoelectrochemical Behavior of a Molecular Ru-Based Water-Oxidation Catalyst Bound to TiO_2-Protected Si Photoanodes. *J. Am. Chem. Soc.* **2017**, *139*, 11345−11348.

(23) Shi, Y.; Hsieh, T.-Y.; Hoque, A.; Cambarau, W.; Narbey, S.; Gimbert-Suriñach, C.; Palomares, E.; Lanza, M.; Llobet, A. High Solar-to-Hydrogen Conversion Efficiency at pH 7 Based on a PV-EC Cell with an Oligomeric Molecular Anode. *ACS Appl. Mater. Interfaces* **2020**, **12**, 55856-55864.

(24) Ye, S.; Ding, C.; Liu, M.; Wang, A.; Huang, Q.; Li, C. Water Oxidation Catalysts for Artificial Photosynthesis. *Adv. Mat.* **2019**, 31, 1902069.

(25) Concepcion, J. J.; Jurss, J. W.; Hoertz, P. G.; Meyer, T. J. Catalytic and Surface-Electrocatalytic Water Oxidation by Redox Mediator-Catalyst Assemblies. *Angew. Chemie - Int. Ed.* **2009**, *48*, 9473-9476.

(26) Assembly, C. R.; Norris, M. R.; Concepcion, J. J.; Fang, Z.; Templeton, J. L.; Meyer, T. J. Low-Overpotential Water Oxidation by a Surface-Bound Ruthenium- Chromophore-Ruthenium-Catalyst Assembly. *Angew. Chem. Int. Ed. Engl.* **2013**, *52*, 13580-13583.

(27) Wu, L.; Nayak, A.; Shao, J.; Meyer, T. J. Crossing the bridge from molecular catalysis to a heterogenous electrode in electrocatalytic water oxidation. Proc. Natl. Acad. Sci. USA **2019**, *116*, 11153-11158.

(28) Chen, Z.; Concepción, J. J.; Jurss, J. W.; Meyer, T. J. Single-Site, Catalytic Water Oxidation on Oxide Surfaces. *J. Am. Chem. Soc.* **2009**, *131*, 15580-15581.

(29) Matheu, R.; Francàs, L.; Chernev, P.; Ertem, M. Z.; Batista, V.; Haumann, M.; Sala, X.; Llobet, A. Behavior of the Ru-bda Water Oxidation Catalyst Covalently Anchored on Glassy Carbon Electrodes. *ACS Catal.* **2015**, *5*, 3422−3429.

(30) Hoque, M. A.; Gil-Sepulcre, M.; de Aguirre, A.; Elemans, J. A. A. W.; Moonshiram, D.; Matheu, R.; Shi, Y.; Benet-Buchholz, J.; Sala, X.; Malfois, M.; Solano, E.; Lim, J.; Garzón-Manjón, A.; Scheu, C.; Lanza, M.; Maseras, F.; Gimbert-Suriñach, C.; Llobet, A. Water Oxidation Electrocatalysis Using Ruthenium Coordination Oligomers Adsorbed on Multiwalled Carbon Nanotubes. *Nat. Chem.* **2020**, *12*, 1060–1066.

(31) Schindler, D.; Gil-Sepulcre, M.; Lindner, J. O.; Stepanenko, V.; Moonshiram, D.; Llobet, A.; Würthner, F. Efficient Electrochemical Water Oxidation by a Trinuclear Ru(bda) Macrocycle Immobilized on Multi-Walled Carbon Nanotube Electrodes. *Adv. Energy Mater.* **2020**, *10*, 2002329.

(32) Creus, J.; Matheu, R.; Peñafiel, I.; Moonshiram, D.; Blondeau, P.; Benet-Buchholz, J.; García-Antón, J.; Sala, X.; Godard, C.; Llobet, A. A Million Turnover Molecular Anode for Catalytic Water Oxidation. *Angew. Chemie Int. Ed.* **2016**, *55*, 15382-15386.

(33) Garrido-Barros, P.; Gimbert- Suriñach, C.; Moonshiram, D.; Picón, A.; Monge, P.; Batista, V. S.; Llobet, A. Electronic I-Delocalization Boosts Catalytic Water Oxidation by Cu(II) Molecular Catalysts Heterogenized on Graphene Sheets. *J. Am. Chem. Soc.* **2017**, *139*, 12907-12910.

(34) Parat, C.; Betelu, S.; Authier, L.; Potin-Gautier, M. Determination of labile trace metals with screen-printed electrode modified by a crown-ether based membrane. *Anal. Chim. Acta* **2006,** *573-574*, 14-19.

(35) Peng, B.; Li, Y.; Zhao, Z.; Chen, Y.; Han, C.C. Facile Surface Modification of PVDF Microfiltration Membrane by Strong Physical Adsorption of Amphiphilic Copolymers. *J. Appl. Polym. Sci.* **2013**, *130*, 3112-3121.

(36) Billon, L.; Gerard, P.; Marcasuzaa, P.; Save, M. Sheets comprising a fluorinated polymer and presenting a variable wettability with respect to a fluid as a function of pH and/or temperature. *WO Patent* 2015170030, **2015.**

(37) Zaouak, O.; Authier, L.; Cugnet, C.; Castetbon, A.; Potin-Gautier, M. Electroanalytical device for cadmium speciation in waters : Development and characterization of a reliable screen-printed sensor. *Electroanalysis* **2010,** *22*, 1151-1158.

(38) Matheu, R.; Neudeck, S.; Meyer, F.; Sala, X.; Llobet, A. Foot of the Wave Analysis for Mechanistic Elucidation and Benchmarking Applications in Molecular Water Oxidation Catalysis. *ChemSusChem* **2016**, *9*, 3361-3369.

(39) Matheu, R.; Ghaderian, A.; Francàs, L.; Chernev, P.; Ertem, M. Z.; Benet-Buchholz, J.; Batista, V. S.; Haumann, M.; Gimbert-Suriñach, C.; Sala, X.; Llobet, A. Behavior of Ru–bda Water-Oxidation Catalysts in Low Oxidation States. *Chem. Eur.J.* **2018**, *24*, 12838-12847.

Table 1. Selected synthetic details and properties of printed electrodes based on MBM/graphite combination prepared in this work

Entry	MBM/Graphite (w%)	Solvent	[MBM] ($g \cdot L^{-1}$)	Nº of printed layer	Conductivity (S/cm)	Thickness (μm)	ΔE_{ox}-E_{red} (V)
1	40% - 60%	mesitylene	100	1	0.79	4.0	1.32
2	40% - 60%	mesitylene	100	2	1.20	7.0	1.34
3	40% - 60%	o-xylene	200	1	2.88	4.5	1.34
4	40% - 60%	o-xylene	200	2	4.17	9.0	1.34
5	30% - 70%	o-xylene	200	1	4.90	7.0	1.32
6	30% - 70%	o-xylene	200	2	6.20	9.0	1.34

*The volume of mesitylene to dissolved 400 mg of MBM was 4.0 ml and need solubilizing time more than 6 h.

*The volume of O-xylene to dissolved 400 mg of MBM was 2.0 ml and need solubilizing time less than 1.30 h.

Table 2. Selected properties of the molecular printed electrodes used in this work.

Cat@CNT@PE	Anchoring strategy.	Support	Experiment	R[a]/Ω	Γ/nmol·cm² before	Γ/nmol·cm² after	TOF s^{-1}	TONs
GC-bda				3-30	12.2			
1-H_2O	π–π	HIPS	CP 25 µA – 225 µA	3.800	0.49	-	1182	92200
15-H_2O	CH-π	Nafion	CP 25 µA – 225 µA	3.000	9.07	5.13	396	7300
			CP 100 µA	3.800	6.13	2.25		15500
			CA 1.45 V	1.200	0.80	0.63		58100
10-$(H_2O)_2$	CH-π	Nafion	CP 25 µA – 225 µA	2.000	0.46	1.28	2646	144800
			CP 100 µA	1.200	3.72	3.48		39800
			CA 1.45 V	4.800	0.95	0.94		53800

* taken after 2 hours exposure.

[a] uncompensated resistance as determined via the iR compensation routine of the CHI potentiostat.

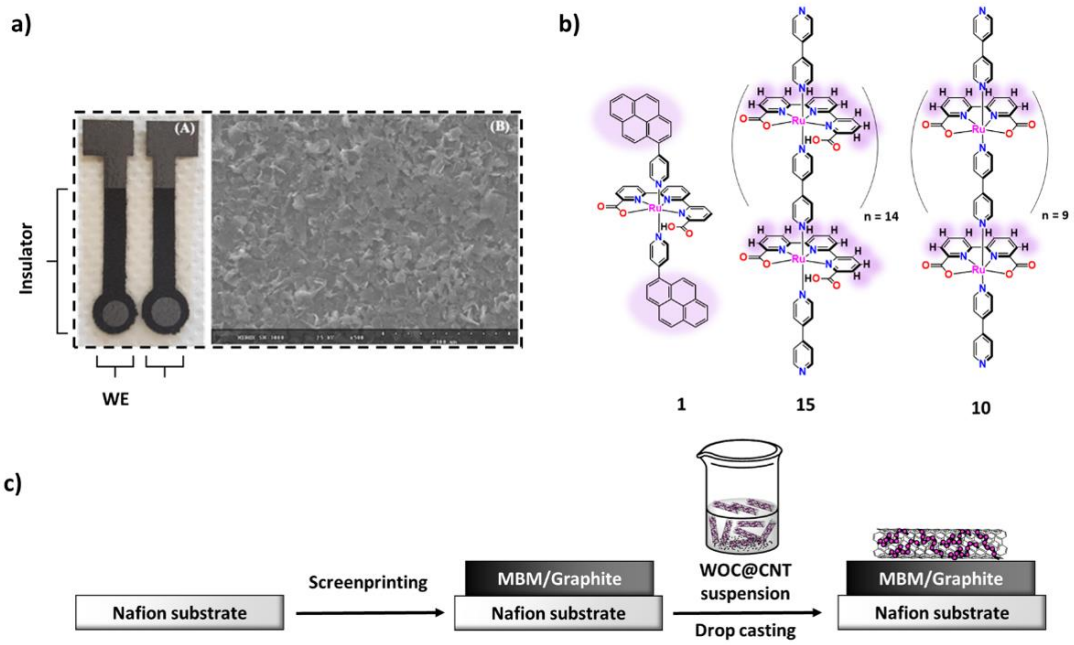

Figure 1. (**A)** picture of the screen-printed electrodes and its SEM image. **(B)** drawing of the molecularly discrete catalyst **1** and oligomers **10** and **15**. **(C)** sequential strategy used for the preparation of molecular printed electrodes MPEs.

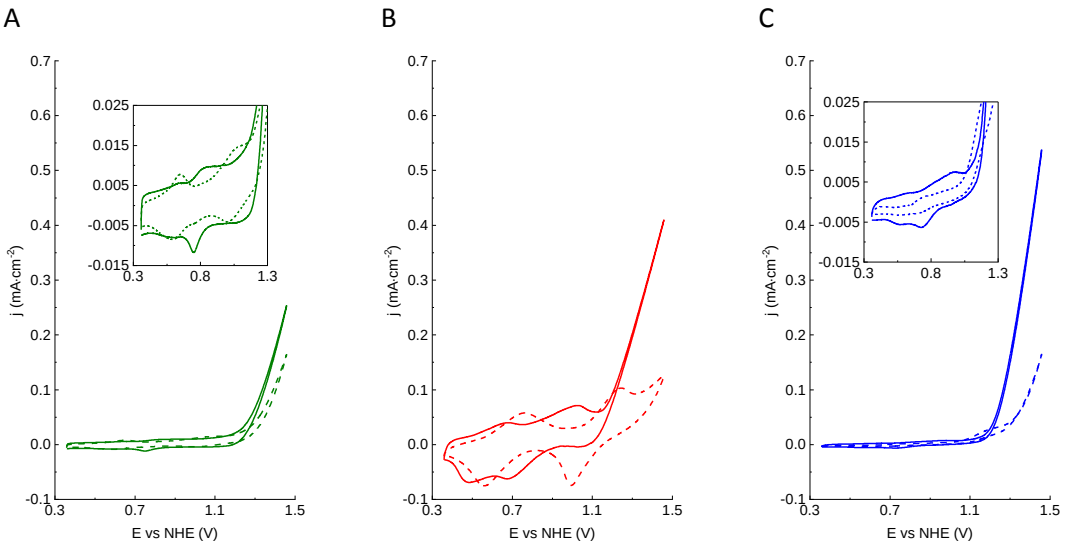

Figure 2. CV experiments of the MPEs recorded in a pH 7 (1.0 M phbf) aqueous solution at a ν = 10 $mV \cdot s^{-1}$ and 1000 Ω iR compensation. **(A) 1@CNT@PE** (green dashed line) and **1-H_2O@CNT@PE** (green solid line); **(B) 15@CNT@PE** (orange dashed line) and **15-H_2O@CNT@PE** (orange solid line); **(C) 10@CNT@PE** (blue dashed line) and **10-$(H_2O)_2$@CNT@PE** (blue solid line). The *inset* in **A** and **C** show the enlargement of the non-catalytic redox waves.

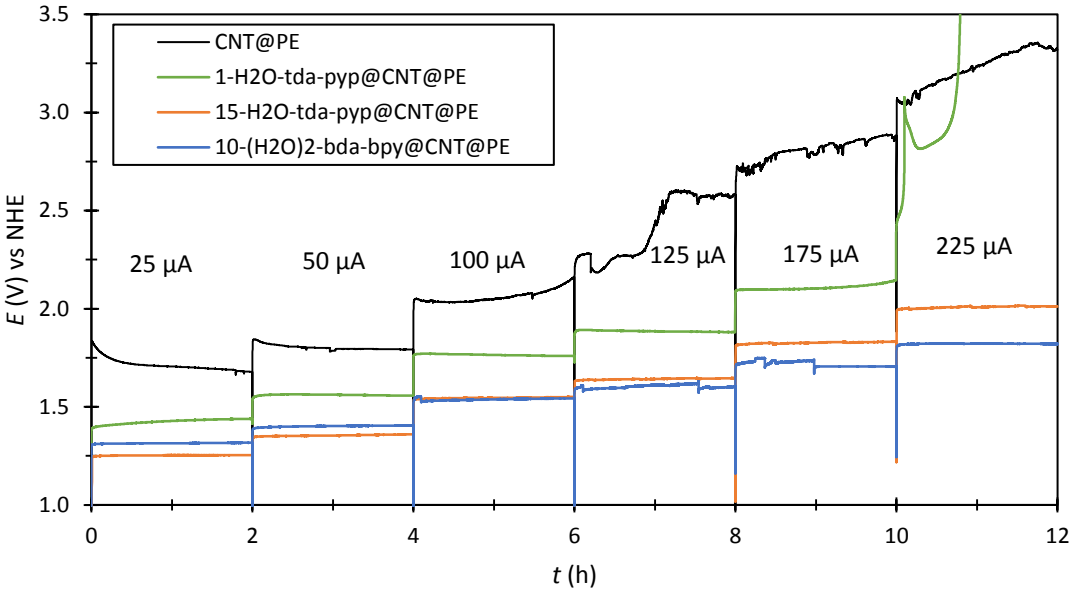

Figure 3. CP of **CNT@PE** (black line), **1-H_2O@CNT@PE** (green line), **10-$(H_2O)_2$@CNT@PE** (blue line) and **15-H_2O@CNT@PE** (red line).

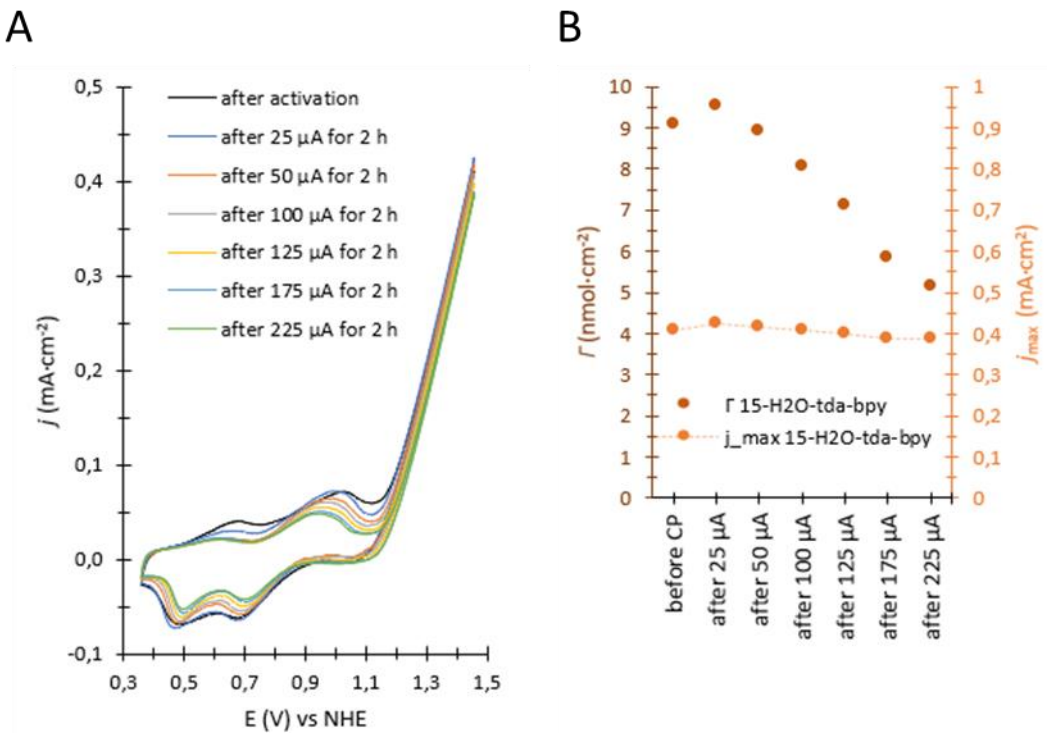

Figure 4. (A) CV evolution of **15-H_2O@CNT@PE** during CPE, taken after each step, in 1.0 M phosphate buffer pH 7 with 10 mV·s^{-1}. **(B)** *Γ* (dark red marks) and j_{max} (orange marks with dashed line) of **15-H_2O@CNT@PE**, obtained from the corresponding CV.

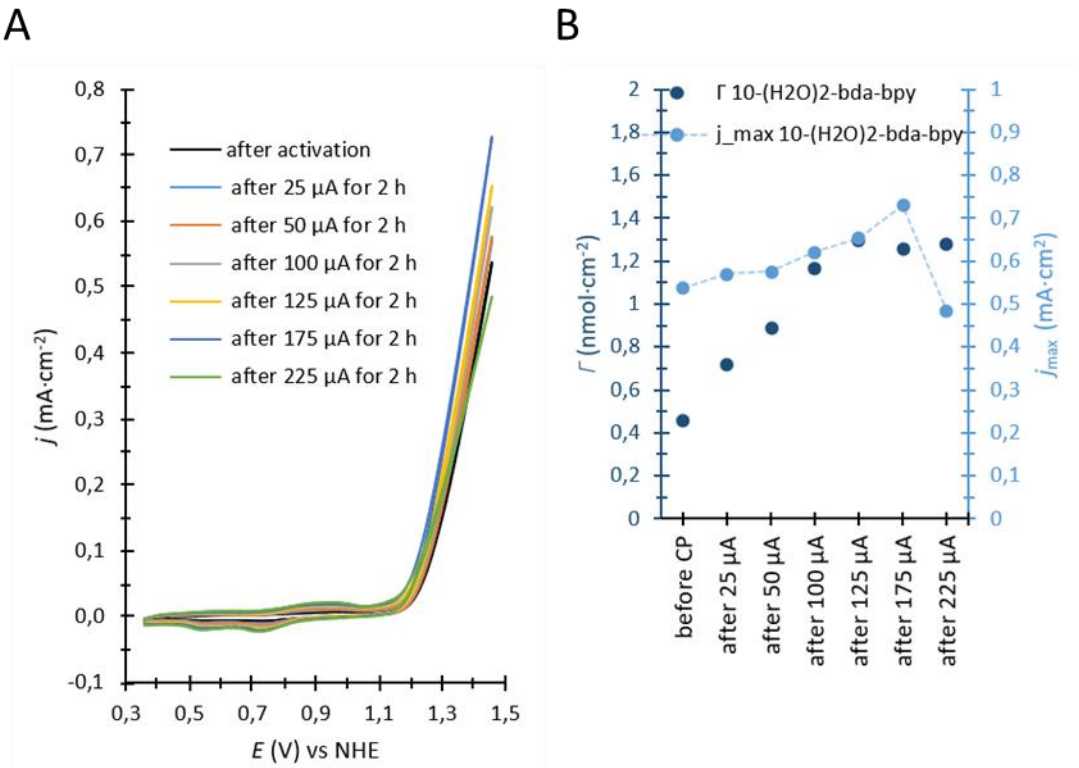

Figure 5. (A) CV evolution of **10-$(H_2O)_2$@CNT@PE** during CP, taken after each CP step, in 1.0 M phbf pH 7 with 10 mV·s^{-1}. **(B)** *Γ* (dark blue marks) and j_{max} (blue marks with dashed line) of **10-$(H_2O)_2$@CNT@PE**, obtained from the corresponding CV.